공학 연구논문집 제 30권 1호 pp. 185~198. 울산대학교
Journal of Engineering Research Vol. 30, No. 1, pp. 185~198. 1999
University of Ulsan

Reactive Flow in Scramjet External Nozzle

Sang-Hyeon Lee
School of Transportation Systems Engineering

<요 약>

비평형 화학반응을 포함한 2차원 Navier-Stoke 방정식과 k-ω 난류모델을 이용하여 단팽창 램프노즐(Single Expansion Ramp Nozzle) 내의 연소 및 추력특성을 연구하였다. 스크램제트엔진의 외부노즐은 대부분의 추력을 생성하기 때문에 중요한 부분 중의 하나이다. 따라서 극초음속항공기에서 요구되는 노즐을 설계하기 위해서는 외부노즐의 추력특성을 정확히 예측할 수 있어야 한다. 외부노즐의 추력특성에 미치는 가장 해석이 어려운 문제는 미연가스가 노즐로 유입되는 것이다. 특히, 노즐의 팽창부에서는 온도가 급격하게 감소하기 때문에 연소 및 재결합반응이 서로 복잡한 형태로 결합되어 발생하므로 이에 대한 규명이 필요하다. 본논문은 노즐의 입구조건의 변화, 즉, 노즐입구에서의 공기와 연료의 온도, 유도구간의 길이, 연료의 수직위치등을 변화시켜면서 연소 및 추력특성을 살펴보았다. 이 과정에서 연소 및 추력특성의 시간진동이 발견되었으며 이에 대한 규명을 시도하였다.

Nomenclature

H	=	Height of inlet plane
M	=	Mach number
p	=	static pressure
T	=	temperature
u, v	=	velocity components
x, y	=	cartesian coordinates
Y	=	mass-fraction
ρ	=	density

Subscript

a	=	air
f	=	fuel

o = stagnation

Introduction

NAL-Kakuda has succeeded the test of M6 scramjet engine in the high altitude test facility (HATF), and has a plan to design external nozzle for scramjet engine[1-2]. The external nozzle is one of the important parts of the scramjet engine, since the external nozzle gives a major portion of thrust. One of the possible candidates for the external nozzle is the single-expanded ramp nozzle (SERN). NAL-Kakuda designed a SERN separately from scramjet combustor and measured the thrust characteristics such as wall pressure, boundary layer loss, divergence-loss and etc[3-6]. Now, NAL-Kakuda is trying to match the external nozzle to scramjet combustor. One of the critical problems of external nozzle is the unburned gas mixture entering the external nozzle from combustor. The first purpose of this study is to find out the flow, reaction and thrust characteristics of the external nozzle (SERN). The second one is to find out the effects of entrance condition of unburned gas mixture on the thrust characteristics.

The entrance conditions of the external nozzle, the outlet conditions of the combustor, have great influences on the burning processes and the thrust characteristics. Three kinds of parametric studies are conducted with varying (1) air temperatures, (2) fuel temperatures and (3) fuel positions. The temperature of fuel-air mixture in the external nozzle is very important since it has great influences on the chemical reaction processes in the external nozzle. The reactions in the external nozzle are dominated by the recombination processes if the temperature of the fuel-air mixture is lower than a critical point, while the reactions are dominated by the fuel consuming processes if the temperature is higher than the critical point. The fuels with different locations at the entrance of external nozzle show different histories of temperature drop during the passage through the expansion waves, which result in different burning and recombination processes. Also, the length of the induction zone has great influences on burning and, in turn, the temperature of the mixture before entering the external nozzle. The influences of these parameters on the flow, chemical reaction and thrust characteristics will be shown in detail.

During the first step of this study, it was found that there are time-oscillations of flow and thrust characteristics in the external nozzle. These time-oscillations are believed to be driven by chemical reactions, especially due to the oscillations between the fuel consumptions and recombinations. In the external nozzle, there are temperature drops after passing through the expansion waves, which initiate recombination processes. The key species for these oscillations are HO_2 and H_2O_2, which are very unstable and have very short existence-time. These species are well known to have strong influences on the ignition and recombination processes. The effects of these

time oscillations of chemical reactions and their influences on the thrust characteristics are investigated in detail, and also the effects of the species HO_2 and H_2O_2, are checked.

Calculations

Geometry and calculation conditions

Although the mixing and combustion process in the external nozzle is three-dimensional, for the purpose of simplicity the effects of lateral dimension are neglected and the nozzle is treated as two-dimensional. The geometry and dimensions of the external nozzle treated in this study are shown in Fig. 1. These dimensions are consistent with the M6 scramjet model of NAL-Kakuda. The expansion angle is 15° and the Aera ratio between nozzle-exit plane and entrance plane is 5. The length of induction zone was varied for the parametric study.

The fuel used in this study is hydrogen. The stagnation pressure, p_0, is 4.5106 Pa and Mach number is 2.0 for air. The pressure and Mach number for air are fixed for all calculations regardless of parametric studies. The static pressure and velocity of fuel are same as those of air, respectively. For the purpose of parametric studies the temperatures of air and fuel, the position of fuel and the length of the induction zone are changed. As the canonical case, the air temperature is 817K (stagnation temperature T_{oa} = 1800K), the velocity of air is about 1710m/s, the fuel maximum temperature is 1200K and the fuel is located near the bottom side. Although the range of air temperature is not wide in case the flight Mach number is fixed, however, the stagnation temperature is changed from 1600K to 1800K just for checking the influences of air temperatures. The fuel temperature is changed to control the fuel burning before entering the external nozzle.

Governing equations

The two-dimensional Navier-Stokes equations with chemical reactions are expressed in the following form[7-8].

$$\frac{\partial Q}{\partial t}+\frac{\partial E}{\partial x}+\frac{\partial F}{\partial y}=\frac{\partial E_v}{\partial x}+\frac{\partial F_v}{\partial y}+W$$

The formulas and data of viscosity, thermal conductivity and binary diffusivity are taken from Reid et al[9]. The data of constant pressure specific heat are taken from the NASA polynomial[10] that covers up to 5000K. The vector W is the source term of the chemical

reactions. The production rate of sth species is expressed in the following form:

$$\dot{\rho}_s = M_s \sum_r (\nu''_{s,r} - \nu'_{s,r}) \left[k_{fr} \prod_s \left(\frac{\rho_s}{M_s} \right)^{\nu'_{s,r}} - k_{br} \prod_s \left(\frac{\rho_s}{M_s} \right)^{\nu''_{s,r}} \right]$$

where ν'_s a ν''_s are the forward and backward reaction coefficients, respectively. The reaction rate constants are expressed in the Arrhenius form and the Arrhenius coefficients are obtained from Jachimowski[11]. Table 1 shows the mechanism of Jachimowski model. The k-w turbulence model equations[12-13] are used to calculate turbulent viscosity. In these equations, a model for dilatation-dissipation term suggested by Wilcox[12] are included to predict the compressibility effects. The turbulent diffusivity and turbulent conductivity are obtained from turbulent viscosity. The turbulent Prandtl number and turbulent Schmidt number are both 0.9[14].

Results

Combustion features in external nozzle

Figure 2 shows the distribution of mass fraction of H2O, which shows the rough features of chemical reactions in the external nozzle. The temperature of air and fuel is 817K(the stagnation temperature is 1800K) and 1200K, respectively. This figure shows, roughly, that the autoignitions occur in the induction zone and the chemical reactions take place in the induction zone and external nozzle. The autoignitions occur only when the fuel temperature of the mixing zone is higher than a critical temperature (about 1050K). If the temperature of the mixing zone is lower than the critical temperature, there is no combustion and, consequently, no thrust augmentation. The fuel regions having more opportunity to meet air stream have stronger autoignition than the other regions: the first and third figures in Fig. 2 shows that the fuel regions near the wall experience weaker ignitions than the regions faced to the free stream. The same figures, however, show that the combustions taking place near the wall in the latter part of the induction zone are stronger than the other regions faced to the free stream. This is believed that the regions near the boundary layer are more favorable due to the fact that fluid motion is relatively slow and temperature is relatively high. At the far field of the entrance plane, the combustions faced to the free stream take place stronger than the regions near the wall. This is due to the fact that the regions faced to the free stream are more favorable to obtain oxidizer than the regions near the wall.

Effects of air temperature

Figure 3 shows the variations of combustion and thrust characteristics with varying the air temperatures, while the fuel temperature is fixed at 1200K. The fuel is located at the bottom side of the entrance plane. The length of induction zone is twice of the inlet height. The air temperatures of the three cases are 728K, 773K and 817K whose stagnation temperatures are 1600K, 1700K and 1800K, respectively.

The first graph of Fig. 3 represents the variation of the fuel consumptions. The fuel consumed for the case with the air temperature of 817K is about 7 % of the total fuel. The fuel flow rates for all cases decay almost linearly until it reach x = 2, where the flows enter through the expansion waves. After that position, the decay of fuel flow rates of all cases come to zero and the OH radical disappear abruptly, which means that the chemical reaction comes to be frozen. The second and third figures represent the same trends. The fact that the flow rates of OH radical come to be zero implies that the chemical reaction comes to be frozen. As the air temperatures increase, the fuel consumption, the OH radical, the water vapor and consequently the thrust increase.

Effects of fuel temperature

Figure 4 shows the variations of combustion and thrust characteristics with varying the fuel temperatures, while the air temperature is fixed at 817K (stagnation temperature is 1800K). The fuel is located at the bottom side of the entrance plane. The length of induction zone is twice of the inlet height. The fuel temperatures of the three cases are 1100K, 1200K and 1400K. If the fuel temperature is lower than 1050K, there was no sensible combustion in such way that the little portion of fuel was consumed and no thrust augmentation was obtained.

The two cases whose fuel temperatures are relatively low show the same trends mentioned in the analysis of Fig.3. The fuel flow rates for these two cases decay almost linearly until it reach x = 2, and after that position, the decay of fuel flow rates come to zero. However, the case of highest fuel temperature, 1400K, shows that the fuel is consumed and the water vapor increases, which means that there is strong chemical reactions in the nozzle. Futhermore, the flow rate of OH radical does not come to be zero, which implies that the chemical reaction takes place relatively strong. This result implies that there would be some criteria for the strong combustion in the nozzle where the fluid temperature decreases rapidly due to the expansion waves. As the fuel temperatures increase, the fuel consumption, the OH radical, the water vapor and consequently the thrust increase.

Effects of fuel location

To clarify the effects of fuel location on the combustion and thrust characteristics,

two kinds of parameters are varied. The first parameter is the vertical location of fuel in the inlet plane and the other one is the length of induction zone (the distance between the inlet plane and the entrance of the external nozzle). The fuel temperature is fixed at 1200K, while the air temperature is fixed at 817K (stagnation temperature is 1800K). In the cases the fuels are located near the walls (top and bottom walls), the fuels are apart from wall surface so that the nearest distance between the wall and fuel is 5 percent of inlet height. Figure 5 and 6 show the variations of combustion and thrust characteristics with variations of the fuel positions; the length of induction zone is twice of inlet height for Fig. 5 (hereafter, short-induction case) and four times of inlet height for Fig. 6 (hereafter, long-induction case). Each combustion and thrust characteristics is presented in the same scale and range.

Comparing two columns of the graphs, it can be easily noticed that the long-induction cases show higher fuel consumption (higher temperature), higher concentration of OH radical and water vapor, and consequently higher thrust than the short-induction cases. Furthermore, the long-induction cases show strong combustion in the external nozzle, while the short-induction cases are frozen. These trends are the same mentioned in the analyses of the case with high fuel temperature (Fig. 4).

The comparisons among the cases with different vertical locations suggest that the bottom case has the strongest combustion: highest fuel consumption, concentration of OH and water vapor, and cosequently highest thrust. This is due to the fact that the bottom case enters lastly through the expansion waves. In the long-induction cases (Fig. 6), the top and bottom cases whose fuels are located near the walls show alomost same trends of combution characteristics after x = 5H. The slope of fuel consumption is linear, the concentration of OH and water vapor increase linearly, while the center case is almost frozen. This suggests that the boundary layers have an important role in the combustion process of external nozzle. The fluid in the boundary layers could maintain relatively high temperature during the expansion since the velocity is small and the temperature is relatively high. This explanation makes it possible to analyze the phenomena that the bottom and top cases show the restart of the combustion after the local frozen zone, between about x = 0 and x = 4. The relatively high temperatures in the boundary layers could make it possible to re-ignite the fuel-air mixture after the temperature drop due to the expansion waves. Because of the same reason, the center case does not show the restart of the strong combustion, since it does not have the fuel-air mixture near the boundary layers.

Time oscillation

There are time-oscillations of the flow and thrust characteristics in the external nozzle. It is believed that these time-oscillations are driven by the interaction between chemical reactions and fluid motions. The oscillations of chemical reactions in the

external nozzle are especially due to the oscillations between the fuel burning and recombinations. In the external nozzle, there are temperature drops after passing through the expansion waves, which initiate recombination processes. The key species for these oscillations are HO_2 and H_2O_2, which are very unstable and have very short existence-time. These species are well known to have strong influences on the ignition and recombination processes. The calculations, during this study, without considering the species HO_2 and H_2O_2 did not show the time oscillations. These time oscillations of chemical reactions results in time oscillations of thrust, which is undesirable situation.

Figure 7 shows the time oscillations of combustion and thrust characteristics. The temperatures of air and fuel are 817K and 1200K, respectively. The center case(left column) shows regular time oscillations of combustion and thrust characteristics, while the bottom case (right column) shows very irregular time oscillations in the far region from the nozzle entrance. The trends of top case are similar to those of bottom case.

In the center case, the periods of all kinds of time oscillations are the same value. There are almost linear phase shifts according to the axial distance. This means that the time oscillations propagate from upstream to downstream. There are the variations of amplitudes according to the axial distance. For the mass flow rate of hydrogen, the amplitude increases until about $x = 0$ where the flow enters through the expansion waves, and after that position the amplitude is maintained. The amplitude of OH radical is large only near the entrance plane ($x = 0$). The amplitude of the thrust increases gradually until about $x = 9$ and after that position decreases.

In the bottom case, the time oscillation of the concentration of OH radical is much stronger and more irregular than that of other characteristics. This suggests that the strong and irregular time oscillations be originated from the time oscillation of the concentration of OH radical. The time oscillation of OH radical is believed to come from the temperature oscillation due to the correlations between temperature drop by flow expansion and wall heating by strong turbulence whose influences are very strong on the chemical reactions.

The exact mechanisms of triggling the time oscillations and the key parameters contolling the oscillations are not fully understood until now. These matters will be studied from now on.

Concluding Remarks

The combustion and thrust characteristics in the single-expanded ramp nozzle (SERN) were studied numerically with two-dimensional Navier-Stokes equations and $k-\omega$ turbulence model.

The autoignitions occur only when the fuel temperature of the mixing zone is higher than a critical temperature (about 1050K). If the temperature of the mixing zone is

lower than the critical temperature, there is no combustion and, consequently, no thrust augmentation. The expansion waves make the temperature drop and the chemical reaction be frozen. As the temperatures of air and fuel increase, the fuel consumption, the OH radical, the water vapor and consequently the thrust increase.

There would be some criteria for the strong combustion in the nozzle where the fluid temperature decreases rapidly due to the expansion waves. If there are strong chemical reactions in the induction zone due to high temperature in the mixture region or long induction zone, there are strong combustion in the external nozzle. The boundary layers have strong effects on the restart of combustion in the external nozzle.

The fuel location in the inlet plane has a great deal of influence on the combustion and thrust characteristics. This is related with the effects of boundary layer mentioned above and the time entering through the expansion waves. Therfore, The bottom case shows the strongest combustion and the largest thrust augmention. The bottom and top cases show stronger combustion and larger thrust augmention.

There are time-oscillations of the flow and thrust characteristics in the external nozzle. The oscillations of chemical reactions in the external nozzle are due to the alternating occurrence of the fuel burning and recombinations. The periods of all kinds of time oscillations are the same value. However, there are almost linear phase shifts and the variations of amplitudes according to the axial distance. The exact mechanisms of initiating the time oscillations and the key parameter contolling the oscillations are not fully understood until now.

Acknowlegements

본 연구는 울산대학교 수송시스템공학부 신진교수연구비의 지원을 통해 이루어졌으며, 저자는 지원에 감사드립니다.

Reference

[1] Mitani, T., Sato, S., Tomioka, S., Kanda, T., Saito, T., Sunami, T., and Tani, K., "Scramjet Engine Testing in Mach 6 Vitiated Air," 7th International Space plane and Hypersonic Systems and Technologies Conference, Nov. 18-22, 1996, AIAA 96-4555.

[2] Hiraiwa, T., Sato, S., Tomioka, S., Shimura, T., Mitani, T., "Testing of a Scramjet Engine Model in Mach 6 Vitiated Air Flow," 35th Aerospace Sciences Meeting and Exhibit, Jan. 6-10, 1997, AIAA 97-0292.

[3] Mitani, T., Ueda, S., Tani, K., Miyajima, H., Matsumoto, M., and Yasu, S.,

"Validation Studies of Scramjet Nozzle Performance," Journal of Propulsion and Power, Vol. 9, No. 5, 1993, pp. 725-730.

[4] Ishiguro, T., Takaki, R., Mitani, T., and Hiraiwa, T., "Three-Dimensional Analysis of Scramjet Nozzle Flow," Journal of Propulsion and Power, Vol. 10, No. 4, 1994, pp. 540-545.

[5] Hiraiwa, T., Tomioka, S., Ueda, S., Mitani, T., Yamamoto, M., and Matsumoto, M., "Performance Validation of Scramjet Nozzle at Various Nozzle Pressure Ratio," Journal of Propulsion and Power, Vol. 11, No. 3, 1995, pp. 403-408.

[6] Miyajima, H., Mitani, T., Sato, S., Ueda, S., Tani, K., Hiraiwa, T., Tanaka, A., Yasu, S., and Higashino, K., "Studies on Scramjet Nozzles (1) Performance of Two Dimensional Nozzle," NAL TR-1149, 1992.

[7] Hirsch, C., Numerical Computation of Internal and External Flows, John Wiley & Sons, New York, 1990, pp. 408-594.

[8] Hoffmann, K. A., Computational Fluid Dynamics for Engineers, Engineering Education

[9] Reid, C. R., Prausnitz, J. M., and Poling, B. E., "The Properties of Gases and Liquids," 4th ed., McGraw-Hill, New York, 1988, pp. 388-631.

[10] Jachimowski, C. J., "An Analytical Study of the Hydrogen-Air Reaction Mechanism with Application to Scramjet Combustion," NASA TR-2791, 1988.

[11] Gardiner, Jr., W. C. , "Combustion Chemistry," Springer-Verlag, New York, 1984, pp. 485-504.

[12] Wilcox, D. C., "Turbulence Modeling for CFD," DCW Industries, 1993, pp. 73-212.

[13] Patel V. C., Rodi, W., and Scheuerer, G., Turbulence Models for Near-Wall and Low Reynolds Number Flows: A Review, *AIAA Journal*, Vol. 23, No. 9, 1985, pp. 1308-1319.

[14] Yungster, S., Numerical Study on Shock-Wave/Boundary Layer Interactions in Premixed Combustible Gases, *AIAA Journal*, Vol. 30, No. 10, 1992, pp. 2379-2387.

Table 1. Hydrogen-Air detailed kinetic mechanism introduced by Jachimowski. This model involves 33 elementary steps and 13 reacting species (H, O, OH, H_2O, H_2, O_2, H_2O_2, HO_2N_2, N, NO, HNO, NO_2). Rate coefficient is expressed in the Arrhenius form: $k = AT^N \exp(-E/RT)$; units are in seconds, moles, cm^3, cal and K

	Reaction	A	N	E
HA1	$H_2 + O_2 \leftrightarrow OH + OH$	1.70×10^{13}	0.00	48,000
HA2	$H + O_2 \leftrightarrow OH + O$	2.60×10^{14}	0.00	16,800
HA3	$O + H_2 \leftrightarrow OH + H$	1.80×10^{10}	1.00	8,900
HA4	$OH + H_2 \leftrightarrow H_2O + H$	2.20×10^{13}	0.00	5,150
HA5	$OH + OH \leftrightarrow H_2O + O$	6.30×10^{12}	0.00	1,090
HA6	$H + OH + M \leftrightarrow H_2O + M$	2.20×10^{22}	-2.00	0
HA7	$H + H + M \leftrightarrow H_2 + M$	6.40×10^{17}	-1.00	0
HA8	$H + O + M \leftrightarrow OH + M$	6.00×10^{16}	-0.60	0
HA9	$H + O_2 + M \leftrightarrow HO_2 + M$	2.10×10^{15}	0.00	-1,000
HB1	$HO_2 + H \leftrightarrow H_2 + O_2$	1.30×10^{13}	0.00	0
HB2	$HO_2 + H \leftrightarrow OH + OH$	1.40×10^{14}	0.00	1,080
HB3	$HO_2 + H \leftrightarrow H_2O + O$	1.00×10^{13}	0.00	1,080
HB4	$HO_2 + O \leftrightarrow O_2 + OH$	1.50×10^{13}	0.00	950
HB5	$HO_2 + OH \leftrightarrow H_2O + O_2$	8.00×10^{12}	0.00	0
HB6	$HO_2 + HO_2 \leftrightarrow H_2O_2 + O_2$	2.00×10^{12}	0.00	0
HC1	$H + H_2O_2 \leftrightarrow H_2 + HO_2$	1.40×10^{12}	0.00	3,600
HC2	$O + H_2O_2 \leftrightarrow OH + HO_2$	1.40×10^{13}	0.00	6,400
HC3	$OH + H_2O_2 \leftrightarrow H_2O + HO_2$	6.10×10^{12}	0.00	1,430
HC4	$H_2O_2 + M \leftrightarrow OH + OH + M$	1.20×10^{17}	0.00	45,500
HC5	$O + O + M \leftrightarrow O_2 + M$	6.00×10^{17}	0.00	-1,800

	Reaction	A	N	E
NA1	$N + N + M \leftrightarrow N_2 + M$	2.80×10^{17}	-0.75	0
NA2	$N + O_2 \leftrightarrow NO + O$	6.40×10^{9}	1.00	6,300
NA3	$N + NO \leftrightarrow N_2 + O$	1.60×10^{13}	0.00	0
NA4	$N + OH \leftrightarrow NO + H$	6.30×10^{11}	0.50	0
NB1	$H + NO + M \leftrightarrow HNO + M$	5.40×10^{15}	0.00	-600
NB2	$H + HNO \leftrightarrow NO + H_2$	4.80×10^{12}	0.00	0
NB3	$O + HNO \leftrightarrow NO + OH$	5.00×10^{11}	0.50	0
NB4	$OH + HNO \leftrightarrow NO + H_2O$	3.60×10^{13}	0.00	0
NB5	$HO_2 + HNO \leftrightarrow NO + H_2O$	2.00×10^{12}	0.00	0
NB6	$HO_2 + NO \leftrightarrow NO_2 + OH$	3.40×10^{12}	0.00	-260
NC1	$H + NO_2 \leftrightarrow NO + O_2$	3.50×10^{14}	0.00	1,500
NC2	$O + NO_2 \leftrightarrow NO + O_2$	1.00×10^{13}	0.00	600
NC3	$NO_2 + M \leftrightarrow NO + O + M$	1.16×10^{16}	0.00	66,000

Third body efficiencies relative to N_2

HA6	$H + OH + M \leftrightarrow H_2O + M$	H_2O=6.0
HA7	$H + H + M \leftrightarrow H_2 + M$	H_2O=6.0, H_2=2.0
HA8	$H + O + M \leftrightarrow OH + M$	H_2O=5.0
HA9	$H + O_2 + M \leftrightarrow HO_2 + M$	H_2O=16.0, H_2=2.0
HC4	$H_2O_2 + M \leftrightarrow OH + OH + M$	H_2O=15.0

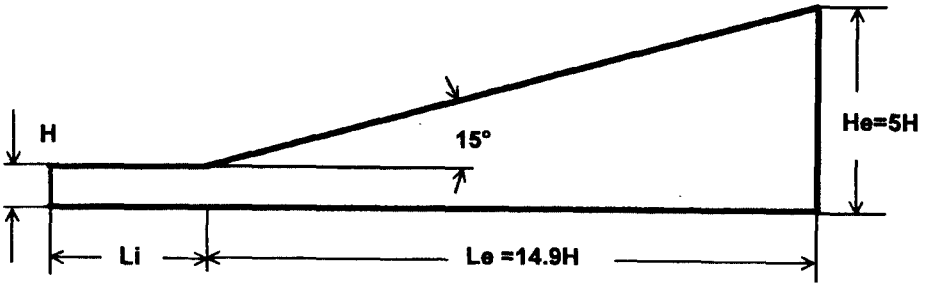

Fig. 1 Geometry of two-dimensional single expansion ramp nozzle (SERN): expansion angle = 15°, H (height of inlet plane) = 250mm, He (height of exit plane) = 5H, Li (length of induction zone) = 2H or 4H, Le (length of nozzle) = 14.9H.

Fig. 2 Distribution of mass fraction of H2O in three different cases: the fuels are located at (a) top (b) center and (c) bottom of the entrance plane, respectively. The maximum mass-fraction of H2O is 0.06. The temperature of air and fuel is 817K and 1200K, respectively. The pressure and velocity of fuel are same with those of air.

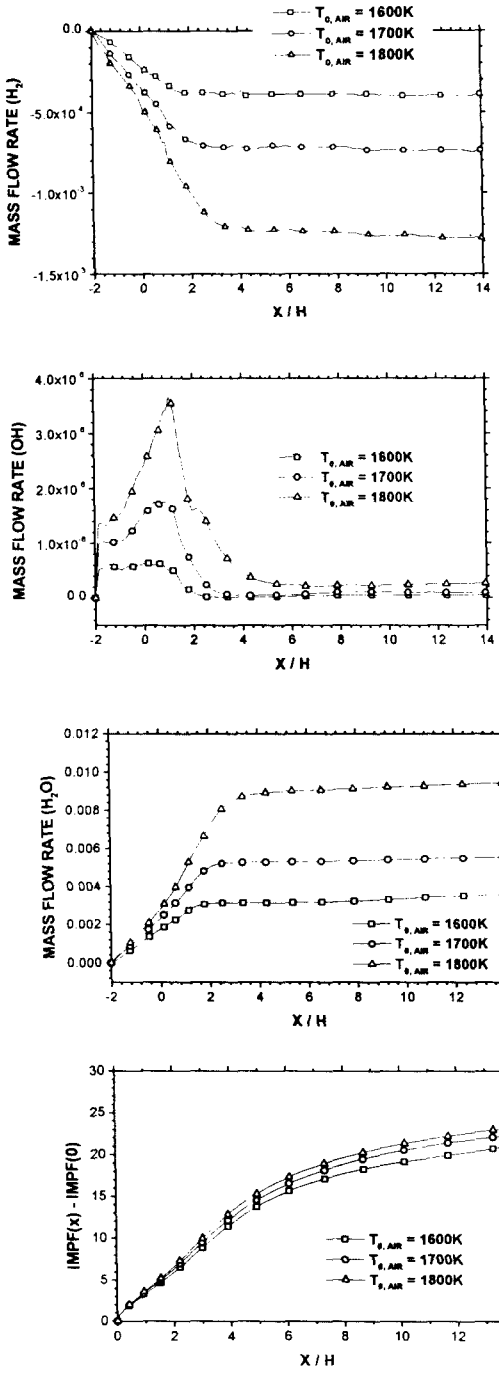

Fig. 3 Effects of air temperature on combustion and thrust characteristics

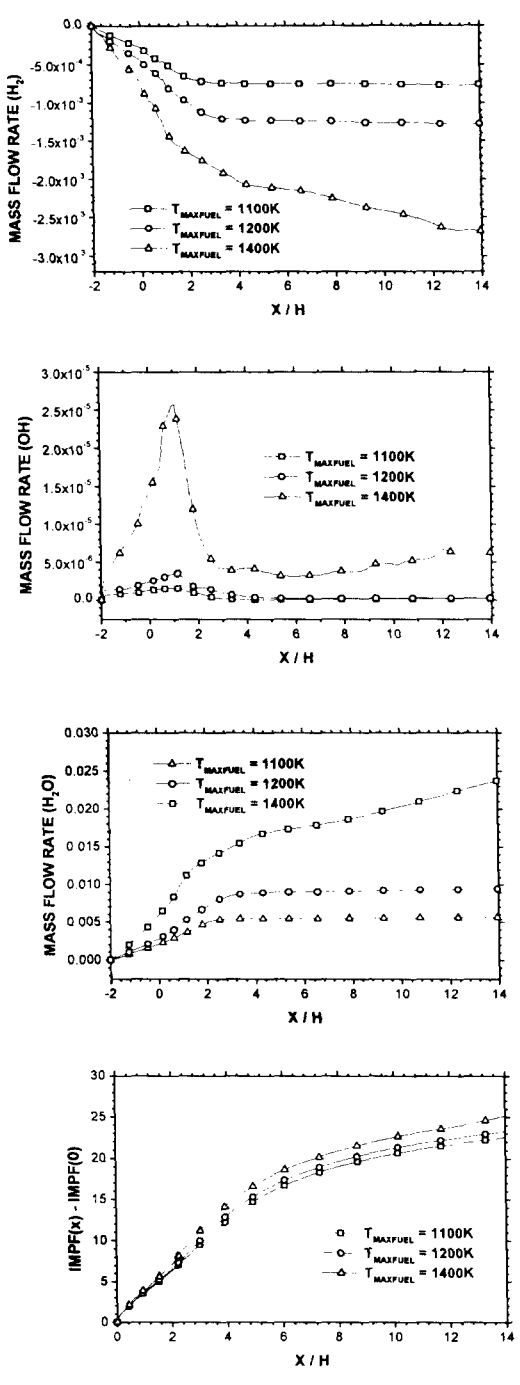

Fig. 4 Effects of fuel temperature on combustion and thrust characteristics

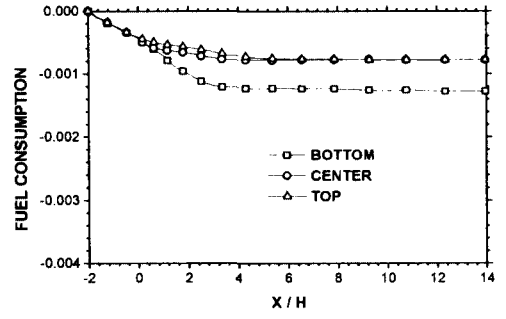

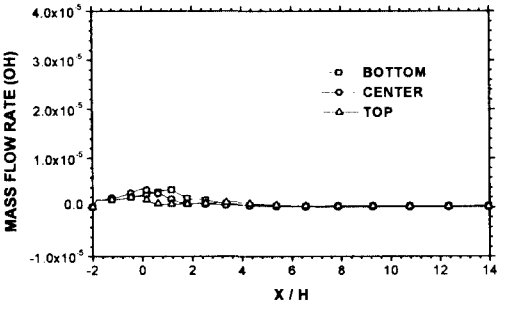

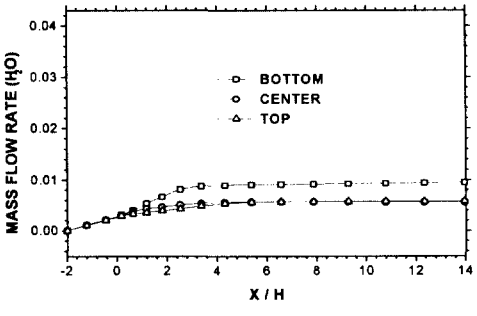

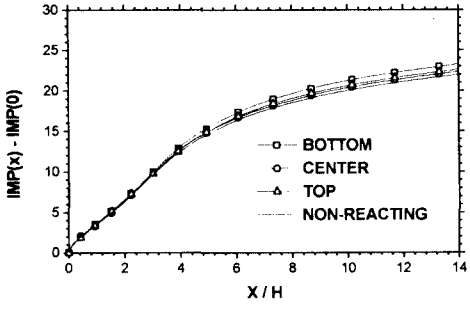

Fig. 5 Effects of fuel position on combustion and thrust characteristics. (Li = 2.0H)

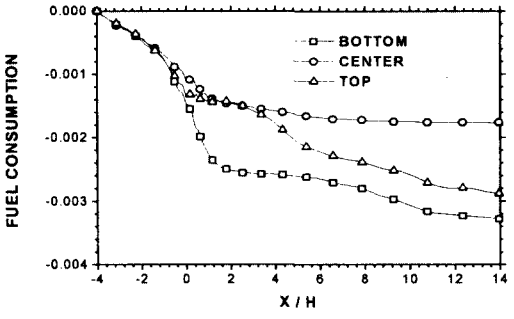

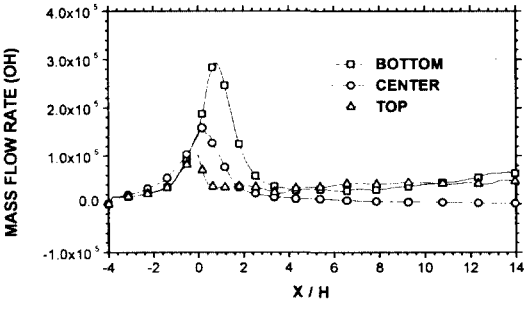

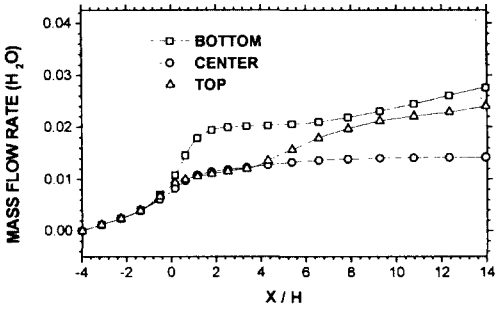

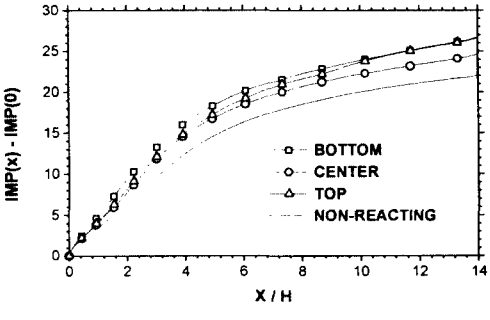

Fig. 6 Effects of fuel position on combustion and thrust characteristics. (Li = 4.0H)

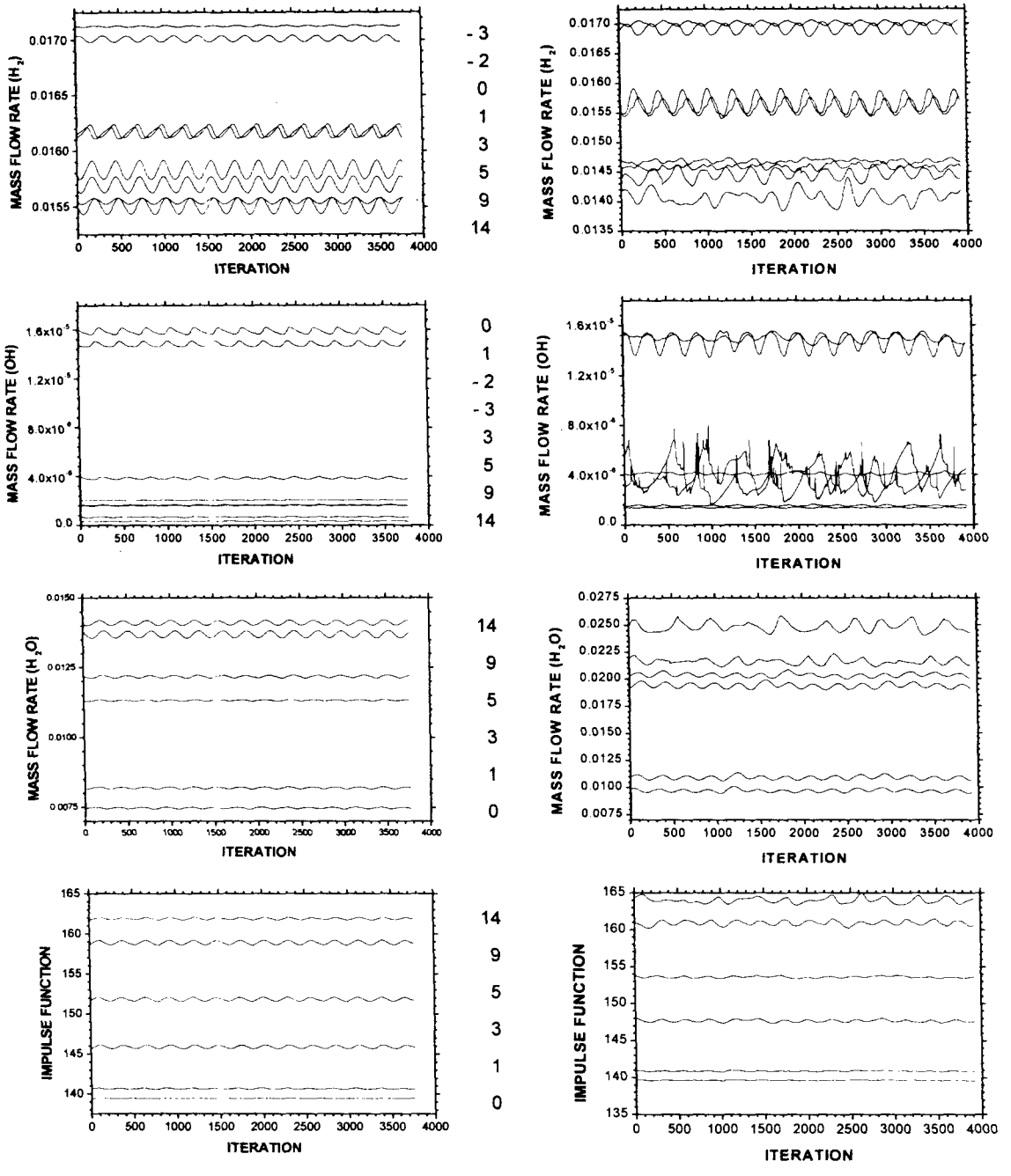

(a) Center Case (b) Bottom Case

Fig. 7 Time oscillations of combustion and thrust characteristics. The numbers at the center column of the graphs mean the axial distance from nozzle entrance plane. The sequence of the number correspond that of the graph lines.